Inorganic Chemistry

pubs.acs.org/IC

Article

Metal-Centered Boron-Wheel Cluster of $Y©B_{11}^{2-}$ with Rare D_{11h} Symmetry

Xin-Ran Dong, Jing-Xuan Zhang, Teng-Teng Chen,* Cong-Qiao Xu,* and Jun Li*

Cite This: *Inorg. Chem.* 2024, 63, 6276−6284

Read Online

ACCESS | Metrics & More | Article Recommendations | Supporting Information

ABSTRACT: Molecules with high point-group symmetry are interesting prototype species in the textbook. As transition metal-centered boron clusters tend to have highly symmetric structures to fulfill multicenter bonding and high stability, new boron clusters with rare point-group symmetry may be viable. Through in-depth scrutiny over the structures of experimentally already observed transition metal-centered boron-wheel complexes, geometric and electronic design principles are summarized, based on which we studied $M©B_{11}^{k-}$ (M = Y, La; Zr, Hf; k = 1, 2) clusters and found that a $Y©B_{11}^{2-}$ boron-wheel complex has an unprecedented D_{11h} point-group symmetry. The remarkable stability of the planar $Y©B_{11}^{2-}$ complex is illustrated via extensive global-minimum structural search as well as comprehensive chemical bonding analyses. Similar to other boron-wheel complexes, the $Y©B_{11}^{2-}$ complex is shown to possess σ and π double aromaticity, indeed following the electronic design principle previously summarized. This new compound is expected to be experimentally identified, which will extend the currently known largest possible planar molecular symmetry and enrich the metal-centered boron-wheel class.

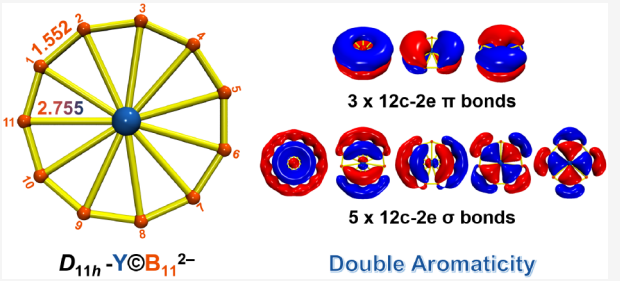

1. INTRODUCTION

Compared with carbon, boron is electron deficient, making boron element displays versatile allotropes with complex crystal structures consisting of different polyhedral cage building blocks.[1,2] A number of boron nanoclusters are found by recent joint photoelectron spectroscopy (PES) and theoretical studies to display a variety of structures and chemical bonding patterns,[3−8] leading to the discoveries of tubular nanostructures,[9,10] all-boron planar monolayers (borophenes),[11,12] bilayer structures,[13] and all-boron cage-like structures (borospherenes).[14,15] Studies on boron−metal clusters have become a new direction of research, discovering new structures such as metal-centered monocyclic wheels,[3] half-sandwiches,[16−18] inverse sandwiches,[19−22] metallo-borophene-like planar structures,[23,24] drum-like metal-doped nanotubular structures,[23,25−28] and metal−boron cage-like structures.[29]

Among the metal boride nanoclusters, the monocyclic metal-centered wheel structures, denoted as $M©B_n^{k-}$,[3] represent a fascinating family of planar boro-metallic clusters that can potentially extend the highest possible planar point-group symmetry. The $Co©B_8^-$ and $Ru©B_9^-$ clusters were the first members of this family.[30] Subsequently, a series of $M©B_n^{k-}$ boro-metallic clusters have been characterized by joint PES and *ab initio* calculations, including $Fe©B_8^-$, $Fe©B_9^-$, $Rh©B_9^-$, $Ir©B_9^-$ and $Re©B_9^-$.[31−33] The $Ta©B_{10}^-$ and $Nb©B_{10}^-$ complexes represent the highest coordination number in the two-dimensional (2D) geometry with perfect D_{10h} symmetry and feature double aromaticity in both in-plane σ and out-of-plane π bonding of the boron ring.[34]

For this rather new class of boron-wheel compounds, geometric and electronic design principles based on σ and π double aromaticity have been proposed by Boldyrev and Wang et al.[3,4,35] First of all, the atomic radius of the central atom must fit the size of the external boron ring in order to facilitate a perfect D_{nh} geometry. In addition, the electronic design principle based on σ and π double aromaticity was proposed to explain the stability of such structures, $M^{(x)}©B_n^{k-}$, where x is the formal valence of the central transition metal atom, n is the number of boron atoms in the monocyclic ring, and k is the charge of the cluster. The design principle requires that the bonding electrons in the system, $3n + x + k$, participate in n two-center two-electron (2c-2e) B−B σ bonds on the edge and two sets of aromatic delocalized bonds (σ and π double aromaticity according to the $4N + 2$ Hückel rule; 12 electrons for six σ and six π electrons or 16 electrons for 10 σ and six π electrons). That is, $3n + x + k = 2n + L$ (L = 12, 16), simplified as $n + x + k = L$ for late and early transition metals, respectively. Previously reported $Ta©B_{10}^-$ and $Nb©B_{10}^-$

Received: December 30, 2023
Revised: March 9, 2024
Accepted: March 14, 2024
Published: March 28, 2024

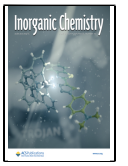

Table 1. Selected Geometric and Electronic Features of Recently Reported $M^{(m)}©B_n^{k-}$ Complexes[a] Compared with our Predicted $Y©B_{11}^{2-}$ Complex[b]

					number of electrons[c]			bond length	
species	n	m	K	$n + m + k$	σ bonds	π bonds	d_{z^2} orbital	B−B	M−B
VB_9^-[d]	9	5	1	15	9	6	0	1.54	2.25
NbB_{10}^-	10	5	1	16	10	6	0	1.52	2.47
TaB_{10}^-	10	5	1	16	10	6	0	1.53	2.47
ReB_8^-[d]	8	7	1	16	8	6	2	1.59	2.17
ReB_9^-	9	7	1	17	10	6	1	1.56	2.27
FeB_8^-[d]	8	8	1	17	10	6	1	1.56	2.07
FeB_9^-	9	8	1	18	10	6	2	1.53	2.23
RuB_9^-	9	8	1	18	10	6	2	1.54	2.25
CoB_8^-	8	9	1	18	10	6	2	1.56	2.03
RhB_9^-[d]	9	9	1	19	10	7	2	1.54	2.26
IrB_9^-[d]	9	9	1	19	10	7	2	1.54	2.26
YB_{11}^{2-}	11	3	2	16	10	6	0	1.55	2.75

[a]For a $M^{(m)}©B_n^{k-}$ complex, m represents the number of the valence electrons of central metal atom, n the number of surrounding boron atoms, and k the negative charge of the cluster. [b]Average bond length is given in Å. [c]Number of electrons represent the number of valence electrons involved in bonding between the central metal atom and the boron wheel. Here we assign the σ bonds for d_{xy}-, $d_{x^2-y^2}$-, and d_{z^2}-M orbitals as delocalized bonding due to the non-negligible contributions of boron. [d]VB_9, ReB_8^-, FeB_8^-, RhB_9^- and IrB_9^- possess quasi-D_{nh} structures because of their mismatching with either the electronic design principle or the geometric design principle.

clusters are typical representatives for early transition metals that comply with this electronic design principle, while $Ru©B_9^-$ and $Co©B_8^-$ are examples for the late transition metals.[30,31,34] So far, only group VB (V, Nb, Ta), group VIB (Re) and group VIIIB (Fe, Ru, Os, Co, Rh, Ir) transition metal elements have been investigated experimentally for their viability to form $M©B_n^{k-}$ molecular wheels with n = 8−10.[30−34] Such metal-centered boron wheels with high coordination numbers have attracted attention from both theorists and experimentalists, as discussed in several recent perspective papers.[36,37] One might then be wondering: do the rest of the transition metal elements, including lanthanides, form $M©B_n^{k-}$-type molecular wheels? What is the highest coordination number for such monocyclic boro-metallic wheels?

So far, molecules with D_{11h} symmetry are extremely rare. To generate the $M©B_n^{k-}$ with an unprecedented D_{11h} symmetry, we target metals in Group III−IV with atomic radii larger than those of Ta and Nb to fit the B_{11} ring according to the geometric design principle. In particular, $Zr©B_{11}^-$, $Hf©B_{11}^-$, $Y©B_{11}^{2-}$ and $La©B_{11}^{2-}$ are potential candidates, as they all have 16 bonding electrons for delocalized bonds. Through quantum chemical investigations, we found that only the $Y©B_{11}^{2-}$ anion is stable and possesses a high D_{11h} symmetry. Various chemical bonding analyses were carried out to understand the stability and electronic structure of this highly symmetry boron cluster. Using global-minimum searches, a perfect planar geometry of YB_{11}^{2-} at the singlet ground state was identified. Further bonding analyses revealed a doubly aromatic external boron ring with five σ and three π delocalized bonds, in both of which the Y center is remarkably involved via its 4d orbitals. IR and UV−vis spectra were simulated for comparison with future experimental characterizations in addition to the electron autodetachment energy and barrier estimated by a semiempirical model.

2. THEORETICAL METHODS

Unbiased structural search for the global minimum of YB_{11}^{2-} with different spin multiplicities was carried out using the TGMin 2.3 package[38−40] based on the Basin-Hopping algorithm.[41] In total, 1500 structures were evaluated by adopting the PBE[42] density functional as implemented in the Gaussian 16 A.03 program, along with cc-pVDZ-PP for Y[43] and cc-pVDZ for B[44] (denoted as PBE/VDZ). The lowest 100 structures were further optimized using PBE0[45] functional with aug-cc-pVTZ-PP for Y and aug-cc-pVTZ for B[43,46] level (denoted as PBE0/aVTZ hereafter), and vibrational frequency calculations were performed at the same level to verify they are true minima. Relative energies of these isomers were refined at the CCSD(T)/def2-TZVP[47] level and the lowest three isomers are selected and reported hereafter. A higher level of theory, CCSD(T)/aVTZ, was used to calculate the energy difference among the three lowest three isomers. Additionally, geometry optimization of singlet YB_{11}^{2-} at the CCSD/aVTZ level was also performed to confirm its D_{11h} geometry.

The local coordinate system (LCS) and energy decomposition analysis combined with natural orbital of chemical valence (ETS-NOCV) analyses[48,49] were performed for the global minimum using ADF 2019.314 at the PBE/TZP level.[50−52] The adaptive natural density partitioning (AdNDP) method[53] was applied to analyze the localized B−B σ bonding and delocalized $Y-B_{11}$ bonding, based on the natural atomic orbital computed by NBO 7.0 program[54] interfaced with Gaussian 16 package at the PBE0/def2-TZVP level of theory. Nucleus-independent chemical shift (NICS)[55] as an aromaticity criterion was calculated using the continuous set of gage transformations (CSGT) method at the PBE0/aVTZ level. The σ and π contributions to $NICS(R)_{zz}$ were calculated using the component of the magnetic shift tensor in the z direction, perpendicular to the plane of the ring, for a dummy atom lying at R (Å) above the plane of the ring.[56] The IR and UV−vis spectra were computed at the PBE0/aVTZ level by using ORCA 4.2.1. The UV−vis spectra were simulated using time-dependent density functional theory (TDDFT) calculations by taking spin−orbit coupling effect into consideration, while the electron−hole distributions were computed and plotted with Multiwfn 3.8.[57] The first vertical detachment energy (VDE_1),which is the energy difference between the ground electronic state of the dianion and that of the monoanion at the same geometry, of the global minimum was calculated at the CCSD(T)/aVTZ level.

3. RESULTS AND DISCUSSION

A brief summary on previously reported transition-metal-centered boron-wheel complexes (see Table 1)[3,4,30−35,58] shows that the B−B bond length is almost independent of the size of boron ring, ranging from 1.52 to 1.59 Å with the majority between 1.53 and 1.56 Å. Thus, the distances between

https://doi.org/10.1021/acs.inorgchem.3c04636
Inorg. Chem. 2024, 63, 6276−6284

the central metal atom and the target boron ring can be approximately estimated using the trigonometric functions, which can help determine the potential existence of metal-centered boron wheels. In terms of the electronic structures, early transition metal boron wheels usually have 16 valence electrons involved in bonding between central metal and the boron wheel, while late transition metal analogs usually have 17 or 18 due to their lower-lying d_{z^2} orbitals. Although the aforementioned electronic design principle successfully explained and summarized the boron-wheel clusters, it shows limitation in directly predicting the maximum boron-ring size for a specific metal atom or the potential metal atom candidates for a given ring size due to the diversity of formal valence for the central metal atom.

In this work, an extended electronic design principle of the $M^{(m)}©B_n^{k-}$ cluster was introduced, in which m is the number of the total valence electrons of the central metal atom, n is the number of boron atoms in the monocyclic ring, and k is the negative charge of the cluster. As a consequence, the total number of valence electrons involved in bonding would be $3n + m + k$. The extended electronic design principle requires that the total number of valence electrons affords n two-center two-electron B−B tangential σ bonds, two sets of aromatic delocalized bonds (10 electrons for σ bonds, six electrons for π bonds) and potential electrons in the d_{z^2} orbital of the central metal atom (up to 2 electrons). Here, the delocalized multicenter two-electron bonds all fulfill the $4N+2$ Hückel rule, with N equal to 2 and 1 for σ and π bonds, respectively. Therefore, $3n + m + k = 2n + L'$ ($L' = 16, 17, 18$) is obligatory. In other words, the number of valence electrons involved in the bonding between boron wheel and metal atom should be 16, 17, or 18 for maximal stability.

From this geometric and electronic design principles, $Zr©B_{11}^-$, $Hf©B_{11}^-$, $Y©B_{11}^{2-}$ and $La©B_{11}^{2-}$ are likely to have suitable atomic radii and 16 valence electrons for delocalized bonding are identified as competent candidates for $M©B_{11}^{k-}$ wheels with D_{11h} symmetry. We hence performed geometry optimizations and vibrational frequency calculations on these candidates, and the results show that the D_{11h} structure is indeed stable for $Y©B_{11}^{2-}$ and $Zr©B_{11}^-$ but is not a local minimum on the potential energy surface for $Hf©B_{11}^-$ or $La©B_{11}^{2-}$. For the $Hf©B_{11}^-$ complex, the external boron ring would fold into a hyperbolic plane, indicating that the metal center is too small to match the 11-membered ring, while $La©B_{11}^{2-}$ suffers from an umbrella-like distortion, suggesting an excessively large metal center, as displayed in Figure S3. As for $Zr©B_{11}^-$, although the D_{11h} structure is indeed a local minimum, it is not the global minimum due to its much higher energy compared with other isomers as shown in Figure S3. Interestingly, $Y©B_{11}^{2-}$, in which the Y metal center has an intermediate atomic radius, is found to adopt a perfect D_{11h} structure as a local minimum, or more precisely speaking, the global minimum, as confirmed by the unbiased search (*vide infra*). We will further examine the stability of this complex and understand its bonding properties in the following sections.

3.1. Global Minimum of YB_{11}^{2-}. To verify that the D_{11h} structure is indeed the global minimum of YB_{11}^{2-}, we performed an extensive global-minimum structural search using density functional theory (DFT) with the TGMin 2.3 package based on randomly seeded structures in two possible spin multiplicities (singlet and triplet).[38−40] In total, 1500 local minima of YB_{11}^{2-} were examined, among which the D_{11h} structure is found to be the most stable singlet species and two low-lying triplet isomers are identified (see Figure 1 and Table S1). As it is difficult to produce singlet−triplet gaps with DFT and the results can vary a lot across different functionals (see Table S2), to further confirm the relative stabilities of different isomers, ab initio coupled cluster calculations have been performed. Energies at the CCSD(T) level verify that the singlet D_{11h}-$Y©B_{11}^{2-}$ structure is indeed the most stable isomer, which adopts a perfectly planar structure with D_{11h} symmetry and a singlet spin state. All other isomers are found to exhibit energies at least 3.86 kcal/mol higher than the D_{11h} one, with those within 20 kcal/mol presented in Figure S1. In particular, the next two lowest-lying isomers adopt triplet spin states with C_s symmetry (isomer II and III in Figure 1).

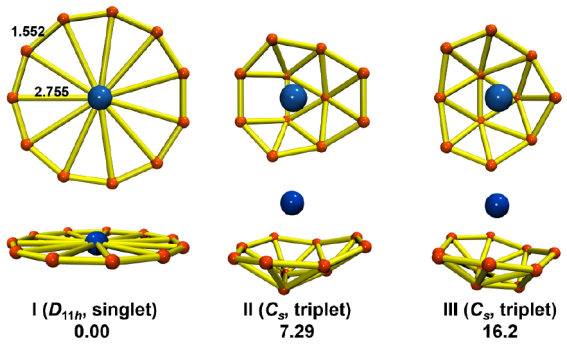

Figure 1. Global minimum (I) and low-lying isomers (II and III) of $Y©B_{11}^{2-}$ along with their point groups, spin states, and relative energies. All energies are in kcal/mol at the CCSD(T)/aVTZ level.

3.2. Chemical Bonding Analyses. *3.2.1. Localized MO Analyses of $Y©B_{11}^{2-}$.* To obtain an in-depth understanding of the electronic structure for the $Y©B_{11}^{2-}$ complex, molecular orbital analyses have been plotted in Figure S4. HOMO−10 to HOMO−5 are all skeletal bonding orbitals within the peripheral boron ring, while HOMO−4 to HOMO show significant Y−B_{11} bonding characters. In particular, the in-plane d_{xy} and $d_{x^2-y^2}$ orbitals of the Y atom are involved in HOMO and HOMO′ while the d_{xz} and d_{yz} orbitals are involved in HOMO−1, HOMO−1′, HOMO−2 and HOMO−2′. The d_{z^2} orbital of Y (mainly LUMO+1) is empty, which is consistent with the extended electronic design principle for the early transition metals. Moreover, there are five occupied in-plane Y−B_{11} bonding orbitals (HOMO−4, HOMO−1, HOMO−1′, HOMO and HOMO′) and three out-of-plane orbitals (HOMO−2, HOMO−2′, HOMO−3), suggesting that the new electronic design principle indeed applies to this system.

The bonding pattern can also be revealed via AdNDP analyses, as shown in Figure 2. By localizing the electron density into multicentered two-electron (nc-2e) bonds, we successfully identified 11 2c-2e B−B σ bonds in the outer B_{11} ring. This is consistent with the fact that the B−B bond length of $Y©B_{11}^{2-}$ is 1.55 Å, close to the B−B bond lengths of previously reported metal-centered boron wheels (Table 1). In addition, two sets of delocalized bonding orbitals have been found, one set with five in-plane skeletal σ bonding orbitals while the other with three out-of-plane π orbitals, both of which satisfy the Hückel's $4N+2$ rule for aromaticity. The enlarged absolute values of $NICS(R)_{zz}$ compared with those of benzene further indicate that $Y©B_{11}^{2-}$ exhibits σ and π aromaticity, as depicted in Figure S5. Thus, the YB_{11}^{2-} dianion

https://doi.org/10.1021/acs.inorgchem.3c04636
Inorg. Chem. 2024, 63, 6276−6284

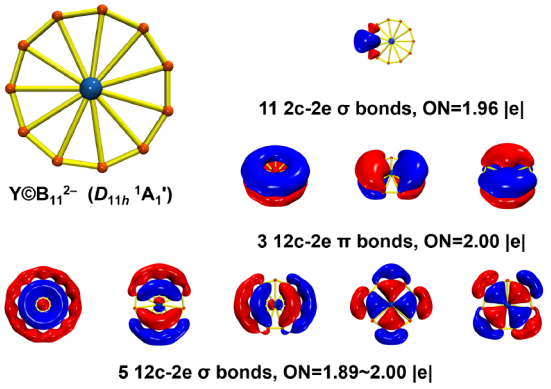

Figure 2. AdNDP analysis for the $Y©B_{11}^{2-}$ dianion at the PBE0/def2-TZVP level. ON represents the occupation number.

demonstrates a doubly aromatic character with the highest planar coordination number (CN = 11) ever known, serving as an extension of the previously reported boron wheels NbB_{10}^- and TaB_{10}^-.

3.2.2. Fragment-Based Bonding Analyses. For a better understanding of the stability of the predicted $Y©B_{11}^{2-}$ complex, the interaction between the metal center and peripheral boron ring is further investigated via a fragment-based approach. As shown in Figure 3, the valence orbitals of

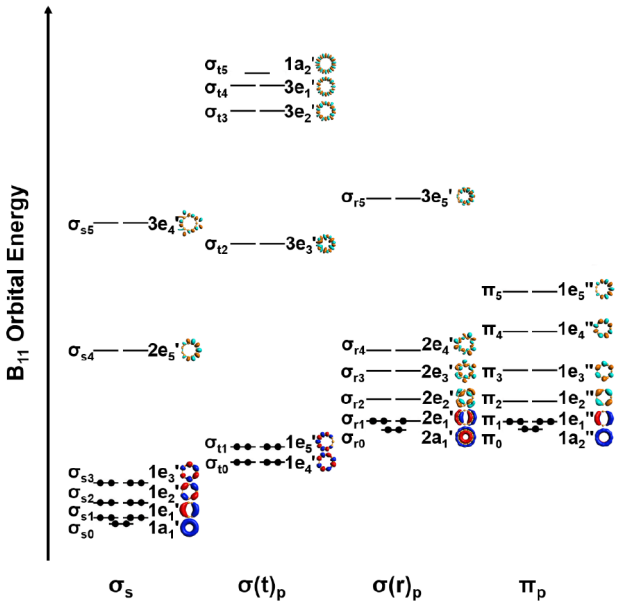

Figure 3. Molecular orbital energy levels of s,p-valence electrons in a local coordinate system (LCS) for isolated B_{11} ring at the PBE0/TZP level, with t and r in parentheses representing tangential and radical direction of the ring using LCS, respectively. Here the p-orbitals are transformed into a LCS as tangential (t), radical (r) and π-type (π), respectively.

the B_{11} ring can be divided into four categories depending on the dominant atomic orbitals, where those for s orbital are denoted as σ_s, tangential p orbital $\sigma(t)_p$, radial p orbital $\sigma(r)_p$, and out-of-plane p_π orbital π_p.[21] Based on the character table of the D_{11h} point group given in Table S3, irreducible representations were assigned for the first time for this novel D_{11h}-symmetry molecule as shown in Figure 3.

By comparison of Figures 2 and 3, the occupied σ_s and $\sigma(t)_p$ orbitals of the B_{11} ring correspond to the 11 B−B σ bonds of $Y©B_{11}^{2-}$. The $\sigma(r)_p$ and π_p orbitals constitute two sets of aromatic bonding patterns, interacting significantly with the central Y atom and forming the bonding MOs by accepting 5 extra electrons in total. Besides, the molecular orbitals of the isolated B_{11} ring and those of the YB_{11}^{2-} complex are closely related. The 5s electrons of Y are promoted to the 4d orbitals due to repulsion with electrons of the boron ring. The HOMO and HOMO′ as well as HOMO−2 and HOMO−2′ of $Y©B_{11}^{2-}$ are derived from the σ_{r2} and π_1 orbitals of B_{11}, respectively, and mix with the corresponding Y 4d orbitals in the same symmetry. As shown in Figure 4, the energy of the σ_{r2}

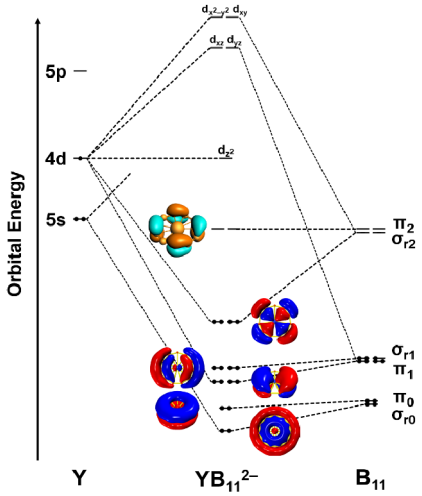

Figure 4. A schematic energy-level correlation diagram of the $Y©B_{11}^{2-}$ cluster.

orbitals is significantly lowered due to the strong orbital overlaps with the Y $4d_{x^2-y^2}$ and $4d_{xy}$ orbitals. The strong orbital interaction leads to a remarkable stabilized HOMO and HOMO′ composing of 17.9% Y 4d and a large energy gap with LUMO and LUMO′. Therefore, according to the electron counting for valence electrons of the B_{11} ring and their orbital interactions with the Y atom, the four electrons in HOMO and HOMO′ can be assigned to the B_{11} ring and the formal oxidation state of the central Y atom should be +3. However, it is interesting to note that when the energy levels of d-type orbitals of the central atom are lower than that of the interacting orbitals of the boron unit, the inverted ligand field interaction will lead to rare low oxidation state of the central metal, which was the case of the unusual oxidation state of Co^{1-} in the late transition metal drum-like complex CoB_{16}^-.[28] Similar LCS analyses can be applied to other boron-wheel complexes in Figure S2, which clearly discloses the interaction pattern between the metal center and the boron ring and reveals the origin of the electronic design principle. Especially noteworthy is that although the π_2 bonding orbital can overlap with central atoms to achieve enhanced stability, it can only interact with f-type atomic orbitals (AOs) due to the orbital symmetry. Additionally, 4f AOs are radially too contracted to participate in effective bonding with boron atoms. Thus, to explore this type of interaction, NpB_{11}^{2-}, PuB_{11}^-, and AmB_{11} boron wheels for 5f elements with total number of 20 valence electrons to fulfill π_2 bonding are constructed. But none of them presents local-minimum D_{11h} geometry without imagi-

https://doi.org/10.1021/acs.inorgchem.3c04636
Inorg. Chem. 2024, 63, 6276−6284

nary frequency. The most promising approach is to build bimetallic group orbitals from d-type AOs, as revealed in the previously reported inverse-sandwich structure $La_2B_n^-$ (n = 7−9).[21]

To further characterize the bonding interaction between the B_{11} ring and Y center, an extended transition state scheme with the theory of natural orbital for chemical valence (ETS-NOCV) was performed. Three fragmentation schemes were taken into consideration, by taking the oxidation state of Y atom as +3, +1, or −1, respectively (see Table 2). Although the Y atom is formally +3 oxidation state in YB_{11}^{2-}, there are significant covalence sharing character that Y^+ presents the smallest orbital interactions and is more favorable to interpret the bonding scheme in ETS-NOCV analysis.[59] Expectedly, the orbital term that contributes the most to the orbital interaction energy comes from the interaction between the σ_{r2} orbital of the boron ring and $4d_{xy}$-, $4d_{x^2-y^2}$-Y orbitals, which accounts for 81.0% of the total orbital interaction (see Figure 4 and Table S4). The orbital interaction is stronger than the attractive electrostatic interaction, suggesting that the interaction between metal center and boron ring is strongly covalent.

Table 2. Calculated ETS-NOCV Results of $Y©B_{11}^{2-}$ with Different Fragment Divisions (a, b, and c) at the PBE/TZP level[a]

fragmentation scheme	A	B	C
Fragment 1	Y^+ ($4d^1_{x^2-y^2}$ and $4d^1_{xy}$)	Y^{3+} ($4d^0_{x^2-y^2}$ and $4d^0_{xy}$)	Y^- ($4d^2_{x^2-y^2}$ and $4d^2_{xy}$)
Fragment 2	B_{11}^{3-} ($\sigma_{r2}^2\pi_2^0$)	B_{11}^{5-} ($\sigma_{r2}^4\pi_2^0$)	B_{11}^- ($\sigma_{r2}^0\pi_2^0$)
ΔE_{int}[b]	−260.59	−1719.15	−324.55
ΔE_{Pauli}[c]	242.92	168.88	815.80
ΔE_{elstat}[d]	−211.96	−1406.42	−476.99
ΔE_{orb}[e]	−291.56	−481.61	−663.36

[a]The energies are given in kcal/mol. [b]ΔE_{int}: Total interaction energy between two fragments. [c]ΔE_{Pauli}: Pauli repulsion energy between two fragments. [d]ΔE_{elstat}: Electrostatic interaction energy between two fragments. [e]ΔE_{orb}: Orbital interaction energy between two fragments.

To summarize, the predicted $Y©B_{11}^{2-}$ complex shows a delocalized, doubly aromatic bonding pattern, as revealed by various bonding analyses. Both the in-plane σ and the out-of-plane π delocalized bonding satisfy Hückel's $4N$+2 rule for aromaticity. In particular, the in-plane bonding between the Y center and the boron ring is essential for increasing the HOMO−LUMO gap and stabilizing the structure.

3.3. Prediction of Spectroscopic Properties. In order to facilitate comparison against future experimental characterizations, we simulated and predicted the IR and UV−vis spectra of $Y©B_{11}^{2-}$ and the previously investigated NbB_{10}^- complex that has similar electron configuration, atomic weight as well as geometric structure (see Figure S6).

The results show that the IR spectra of YB_{11}^{2-} and NbB_{10}^- indeed feature a similar pattern, with only three major peaks due to the high symmetry of the complexes. The strongest peaks of both complexes correspond to an out-of-plane A_2'' vibration of the metal atom. The second peaks in the range of 200 to 400 cm^{-1} correspond to the in-plane vibration of the central atom and the third ones above 600 cm^{-1} correspond to the asymmetrical distortion of the boron wheel. Compared with NbB_{10}^-, the red shift of YB_{11}^{2-} could be explained by the larger radius of the ring and thus relatively weaker radial bonding despite the lighter atomic weight of the Yttrium center.

When it comes to the UV−vis spectra, however, these two complexes have fundamentally different excitation modes despite their similar shape of absorption curves. To characterize the nature of each excitation mode, electron−hole densities are plotted for the major absorption peaks (see Table S5).[60] It can be seen that all excitations of YB_{11}^{2-} have strong Rydberg characters, with the hole density located close to the nuclei and electron density distributed much farther. On the other hand, the primary peak of NbB_{10}^- complex belongs to Rydberg excitation while its secondary peak is valence excitation. In particular, the electron−hole distributions of the two dominant peaks of YB_{11}^{2-} exhibit angular modes, leading to the double degeneracy of each peak, whereas those of NbB_{10}^- show excitation patterns parallel to or perpendicular to the molecular plane.

3.4. Predicted Photoelectron Spectroscopic Properties of YB_{11}^{2-}. Electron detachment energy is an essential molecular property that can be measured by photoelectron spectroscopy. For dianionic species, electron detachment could be thermodynamically favored, because of the Coulomb repulsion within the dianion. Calculation of the electron detachment energy is thus important to estimate the stability of the complex and to compare against future experimental characterizations.

In our study, high-level CCSD(T)/aVTZ calculations reveal that electron detachment of the YB_{11}^{2-} complex is indeed thermodynamically favored, with the calculated electron detachment energy of −0.28 eV (VDE_1), which is reminiscent of previous observation of negative electron-detachment energy in gaseous $[CuPc(SO_3)_4]^{4-}$.[61] Besides, the energy of HOMO will be negative after either considering the solvent effect through the SMD model or setting two positive charges on the eight vertices of a cube evenly to roughly simulate the condition in a crystal lattice. The global-minimum structural search shows that in a nonpolar solvent like benzene, the D_{11h} structure is still the most stable configuration of YB_{11}^{2-} with an enlarged VDE_1 of 2.25 eV, indicating that experimental preparation of this structure is not impossible.

To further verify the stability of the YB_{11}^{2-} complex in the gas phase, we put forward a semiempirical model to estimate its repulsive Coulomb barrier (RCB). Obviously, a long-range repulsive Coulomb interaction exists between the detaching electron and the remaining YB_{11}^- anion, which is proportional to the inverse of distance between the detaching electron and molecular center. On the other hand, in short distance the electron would be tied to the HOMO of the complex. This effect, despite its quantum nature, can be approximated by an exponential decaying term to describe the attraction due to chemical bonding. The Gaussian function is assumed in our model to maintain computational feasibility.

We therefore obtained the following semiclassical potential energy curve for the electron detachment process, with two empirical parameters to be determined:

$$E_{tot} = E_{rep} + E_{attr} = \frac{1}{r} - c \cdot e^{-\alpha r^2}$$

where E_{tot} represents the overall interaction between YB_{11}^- and e^-, E_{rep} and E_{attr} represent the long-range electrostatic repulsion and short-range 'bonding' attraction, respectively.

Such a potential energy curve will lead to an equilibrium distance because of the competition between short-distance

https://doi.org/10.1021/acs.inorgchem.3c04636
Inorg. Chem. 2024, 63, 6276−6284

attraction and long-distance repulsion. We take the radius of the B_{11} ring as an approximate equilibrium distance because the electron should be localized close to the ring at the equilibrium distance. Together with the energy of the equilibrium structure from *ab initio* calculations, we would be able to obtain the following equations that uniquely determine the two empirical parameters:

$$E_{tot}(r_0) = \frac{1}{r_0} - c \cdot e^{-\alpha r_0^2} = E_0$$

$$\left.\frac{dE_{tot}}{dr}\right|_{r=r_0} = -\frac{1}{r_0^2} + c \cdot e^{-\alpha r_0^2} \cdot 2\alpha r_0 = 0$$

where E_0 = 0.28 eV is the energy of the YB_{11}^{2-} complex at the equilibrium distance (r_0 = 2.755 Å) with respect to its self-detachment product ($r = \infty$).

Using this semiempirical model, the repulsive Coulomb barrier can be easily estimated by locating the turning point of the potential energy curve, which was found to be 1.51 eV for the YB_{11}^{2-} system (see Figure 5). This is much higher than the

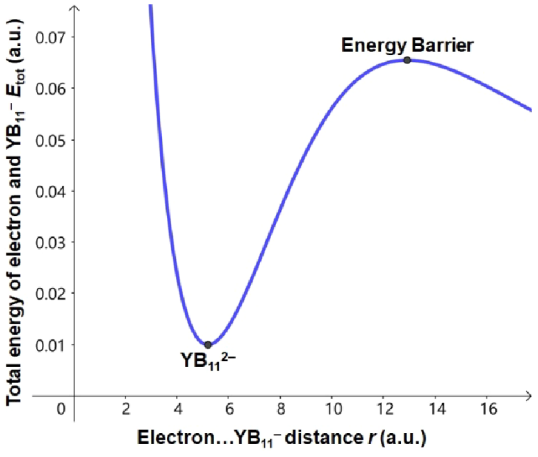

Figure 5. Total energy of the electron and YB_{11}^- as a function of the distance between the electron and YB_{11}^- (r).

energy released in the self-detachment procedure (0.28 eV), which again demonstrates the stability of our predicted complex. Actually, experimental existence of multiply charged anions (MCAs) with repulsive Coulomb barrier and negative VDE_1 have been proved previously.[61−68] Additionally, geometrical size of YB_{11}^{2-} complex is much larger than the previously reported stable gaseous $PtCl_4^{2-}$ with similar electron detachment energy (−0.25 ± 0.05 eV),[62] further indicating that the possibility of experimental detection of YB_{11}^{2-} complex cannot be excluded. Therefore, this YB_{11}^{2-} dianion is metastable because of the repulsive Coulomb barrier for electron emission procedure and can be likely detected in PES spectra.

4. CONCLUSIONS

In conclusion, we have predicted the existence of highly symmetric metal-centered boron-wheel molecule $Y©B_{11}^{2-}$ in unprecedented D_{11h} point-group symmetry by DFT and *ab initio* quantum chemistry calculations. The global-minimum search shows that the singlet D_{11h} A_1' structure is more stable than the other isomers. The D_{11h}-$Y©B_{11}^{2-}$ dianion is found to satisfy the geometric design principle for a metal-centered boron wheel due to the suitable atomic radius of Yttrium, and also fulfills the electronic design principle that ensures the double (σ and π) aromaticity. In addition to 11 2c-2e B−B σ bonds in the B_{11} ring, 5 in-plane σ and 3 out-of-plane π delocalized orbitals are found, both of which satisfy the Hückel's $4N+2$ rule for aromaticity. Besides, strong in-plane σ bonding interaction between the σ_{r2} orbitals of the boron ring and 4d orbitals of Y atom is responsible for the large HOMO−LUMO gap and stability of the $Y©B_{11}^{2-}$ structure. Chemical bonding analysis reveals the strong covalent interaction between the Y center and the external boron ring. For comparison against future experimental characterizations, we calculate its IR and UV−vis spectra as well as the photoelectron spectroscopic properties of this complex. The repulsive Coulomb barrier is estimated via a novel semiempirical model, which can be potentially applied to other multiply charged species. The unprecedented D_{11h}-$Y©B_{11}^{2-}$ structure expands the current boundary of point-group theory in chemistry, and we hence anticipate experimental synthesis and characterization of this complex in the recent future.

■ ASSOCIATED CONTENT

Supporting Information

The Supporting Information is available free of charge at https://pubs.acs.org/doi/10.1021/acs.inorgchem.3c04636.

Structures and relative energies of isomers of $Y©B_{11}^{2-}$; the schematic diagram of LCS analysis on isolated B_6 to B_{11} boron rings; the coordinates of three low-lying isomers of $Y©B_{11}^{2-}$; the canonical MO plots and ETS-NOCV results of $Y©B_{11}^{2-}$; the UV−vis spectra and electron−hole graphs of $Y©B_{11}^{2-}$ and $Nb©B_{10}^-$; the group table of D_{11h} point-group symmetry (PDF)

■ AUTHOR INFORMATION

Corresponding Authors

Teng-Teng Chen − *Department of Chemistry, The Hong Kong University of Science and Technology (HKUST), Clear Water Bay, Hong Kong SAR 999077, China; HKUST Shenzhen-Hong Kong Collaborative Innovation Research Institute, Shenzhen 518045, China*; Email: tengtengchen@ust.hk

Cong-Qiao Xu − *Department of Chemistry and Guangdong Provincial Key Laboratory of Catalytic Chemistry, Southern University of Science and Technology, Shenzhen 518055, China*; orcid.org/0000-0003-4593-3288; Email: xucq@sustech.edu.cn

Jun Li − *Department of Chemistry and Guangdong Provincial Key Laboratory of Catalytic Chemistry, Southern University of Science and Technology, Shenzhen 518055, China; Department of Chemistry and Engineering Research Center of Advanced Rare-Earth Materials of Ministry of Education, Tsinghua University, Beijing 100084, China; Fundamental Science Center of Rare Earths, Ganjiang Innovation Academy, Chinese Academy of Sciences, Ganzhou 341000, China*; orcid.org/0000-0002-8456-3980; Email: junli@tsinghua.edu.cn

Authors

Xin-Ran Dong − *Department of Chemistry and Guangdong Provincial Key Laboratory of Catalytic Chemistry, Southern University of Science and Technology, Shenzhen 518055, China*

https://doi.org/10.1021/acs.inorgchem.3c04636
Inorg. Chem. 2024, 63, 6276−6284

Jing-Xuan Zhang − *Department of Chemistry and Guangdong Provincial Key Laboratory of Catalytic Chemistry, Southern University of Science and Technology, Shenzhen 518055, China;* orcid.org/0000-0002-1358-2789

Complete contact information is available at: https://pubs.acs.org/10.1021/acs.inorgchem.3c04636

Notes

The authors declare no competing financial interest.

■ ACKNOWLEDGMENTS

This work was financially supported by the National Natural Science Foundation of China (Grant 22033005 and 22103035), National Key Research and Development Project (2022YFA1503900 and 2023YFA1506600), Special Funds for the Cultivation of Guangdong College Students' Scientific and Technological Innovation ("Climbing Program" Special Funds, pdjh2020c0032) and partially sponsored by the Guangdong Provincial Key Laboratory of Catalysis (No. 2020B121201002), the Project of Hetao Shenzhen-Hong Kong Science and Technology Innovation Cooperation Zone (HZQB-KCZYB-2020083) and Young Elite Scientists Sponsorship Program by CAST (2023QNRC001). Computational resources were supported by the Center for Computational Science and Engineering at Southern University of Science and Technology, CHEM high-performance supercomputer cluster (CHEM-HPC) and Tsinghua National Laboratory for Information Science and Technology.

■ REFERENCES

(1) Albert, B.; Hillebrecht, H. Boron: Elementary Challenge for Experimenters and Theoreticians. *Angew. Chem. Int. Ed.* **2009**, *48* (46), 8640−8668.

(2) Oganov, A. R.; Chen, J.; Gatti, C.; Ma, Y.; Ma, Y.; Glass, C. W.; Liu, Z.; Yu, T.; Kurakevych, O. O.; Solozhenko, V. L. Ionic high-pressure form of elemental boron. *Nature* **2009**, *457* (7231), 863−867.

(3) Romanescu, C.; Galeev, T. R.; Li, W.-L.; Boldyrev, A. I.; Wang, L.-S. Transition-Metal-Centered Monocyclic Boron Wheel Clusters ($M©B_n$): A New Class of Aromatic Borometallic Compounds. *Acc. Chem. Res.* **2013**, *46* (2), 350−358.

(4) Romanescu, C.; Galeev, T. R.; Li, W.-L.; Boldyrev, A. I.; Wang, L.-S. Geometric and electronic factors in the rational design of transition-metal-centered boron molecular wheels. *J. Chem. Phys.* **2013**, *138* (13), 134315.

(5) Li, W.-L.; Chen, X.; Jian, T.; Chen, T.-T.; Li, J.; Wang, L.-S. From planar boron clusters to borophenes and metalloborophenes. *Nat. Rev. Chem.* **2017**, *1* (10), 0071.

(6) Li, W.-L.; Hu, H.-S.; Zhao, Y.-F.; Chen, X.; Chen, T.-T.; Jian, T.; Wang, L.-S.; Li, J. Recent progress on the investigations of boron clusters and boron-based materials (I): borophene. *Sci. Sin. Chim.* **2018**, *48* (2), 98−107.

(7) Jian, T.; Chen, X.; Li, S.-D.; Boldyrev, A. I.; Li, J.; Wang, L.-S. Probing the structures and bonding of size-selected boron and doped-boron clusters. *Chem. Soc. Rev.* **2019**, *48* (13), 3550−3591.

(8) Chen, T.-T.; Cheung, L. F.; Wang, L.-S. Probing the Nature of the Transition-Metal-Boron Bonds and Novel Aromaticity in Small Metal-Doped Boron Clusters Using Photoelectron Spectroscopy. *Annu. Rev. Phys. Chem.* **2022**, *73* (1), 233−253.

(9) Kiran, B.; Bulusu, S.; Zhai, H.-J.; Yoo, S.; Zeng, X. C.; Wang, L.-S. Planar-to-tubular structural transition in boron clusters: B_{20} as the embryo of single-walled boron nanotubes. *Proc. Natl. Acad. Sci. U.S.A.* **2005**, *102* (4), 961−964.

(10) Oger, E.; Crawford, N. R. M.; Kelting, R.; Weis, P.; Kappes, M. M.; Ahlrichs, R. Boron Cluster Cations: Transition from Planar to Cylindrical Structures. *Angew. Chem. Int. Ed.* **2007**, *46* (44), 8503−8506.

(11) Li, W.-L.; Chen, Q.; Tian, W.-J.; Bai, H.; Zhao, Y.-F.; Hu, H.-S.; Li, J.; Zhai, H.-J.; Li, S.-D.; Wang, L.-S. The B_{35} Cluster with a Double-Hexagonal Vacancy: A New and More Flexible Structural Motif for Borophene. *J. Am. Chem. Soc.* **2014**, *136* (35), 12257−12260.

(12) Piazza, Z. A.; Hu, H.-S.; Li, W.-L.; Zhao, Y.-F.; Li, J.; Wang, L.-S. Planar hexagonal B_{36} as a potential basis for extended single-atom layer boron sheets. *Nat. Commun.* **2014**, *5* (1), 3113.

(13) Chen, W.-J.; Ma, Y.-Y.; Chen, T.-T.; Ao, M.-Z.; Yuan, D.-F.; Chen, Q.; Tian, X.-X.; Mu, Y.-W.; Li, S.-D.; Wang, L.-S. B_{48}^-: A bilayer boron cluster. *Nanoscale* **2021**, *13* (6), 3868−3876.

(14) Zhai, H.-J.; Zhao, Y.-F.; Li, W.-L.; Chen, Q.; Bai, H.; Hu, H.-S.; Piazza, Z. A.; Tian, W.-J.; Lu, H.-G.; Wu, Y.-B.; Mu, Y.-W.; Wei, G.-F.; Liu, Z.-P.; Li, J.; Li, S.-D.; Wang, L.-S. Observation of an all-boron fullerene. *Nat. Chem.* **2014**, *6* (8), 727−731.

(15) Chen, Q.; Li, W.-L.; Zhao, Y.-F.; Zhang, S.-Y.; Hu, H.-S.; Bai, H.; Li, H.-R.; Tian, W.-J.; Lu, H.-G.; Zhai, H.-J.; Li, S.-D.; Li, J.; Wang, L.-S. Experimental and Theoretical Evidence of an Axially Chiral Borospherene. *ACS Nano* **2015**, *9* (1), 754−760.

(16) Popov, I. A.; Li, W.-L.; Piazza, Z. A.; Boldyrev, A. I.; Wang, L.-S. Complexes between Planar Boron Clusters and Transition Metals: A Photoelectron Spectroscopy and Ab Initio Study of CoB_{12}^- and RhB_{12}^-. *J. Phys. Chem. A* **2014**, *118* (37), 8098−8105.

(17) Chen, T.-T.; Li, W.-L.; Jian, T.; Chen, X.; Li, J.; Wang, L.-S. PrB_7^-: A Praseodymium-Doped Boron Cluster with a Pr^{II} Center Coordinated by a Doubly Aromatic Planar η^7-B_7^{3-} Ligand. *Angew. Chem. Int. Ed.* **2017**, *56* (24), 6916−6920.

(18) Li, W.-L.; Chen, T.-T.; Chen, W.-J.; Li, J.; Wang, L.-S. Monovalent lanthanide(I) in borozene complexes. *Nat. Commun.* **2021**, *12* (1), 6467.

(19) Li, W.-L.; Xie, L.; Jian, T.; Romanescu, C.; Huang, X.; Wang, L.-S. Hexagonal Bipyramidal $[Ta_2B_6]^{-/0}$ Clusters: B_6 Rings as Structural Motifs. *Angew. Chem. Int. Ed.* **2014**, *53* (5), 1288−1292.

(20) Li, W.-L.; Chen, T.-T.; Xing, D.-H.; Chen, X.; Li, J.; Wang, L.-S. Observation of highly stable and symmetric lanthanide octa-boron inverse sandwich complexes. *Proc. Natl. Acad. Sci. U.S.A.* **2018**, *115* (30), No. E6972−E6977.

(21) Chen, T.-T.; Li, W.-L.; Li, J.; Wang, L.-S. $[La(\eta^x\text{-}B_x)La]^-$ (x = 7−9): A new class of inverse sandwich complexes. *Chem. Sci.* **2019**, *10* (8), 2534−2542.

(22) Jiang, Z.-Y.; Chen, T.-T.; Chen, W.-J.; Li, W.-L.; Li, J.; Wang, L.-S. Expanded Inverse-Sandwich Complexes of Lanthanum Borides: $La_2B_{10}^-$ and $La_2B_{11}^-$. *J. Phys. Chem. A* **2021**, *125* (12), 2622−2630.

(23) Jian, T.; Li, W.-L.; Chen, X.; Chen, T.-T.; Lopez, G. V.; Li, J.; Wang, L.-S. Competition between drum and quasi-planar structures in RhB_{18}^-: Motifs for metallo-boronanotubes and metallo-borophenes. *Chem. Sci.* **2016**, *7* (12), 7020−7027.

(24) Li, W.-L.; Jian, T.; Chen, X.; Chen, T.-T.; Lopez, G. V.; Li, J.; Wang, L.-S. The Planar CoB_{18}^- Cluster as a Motif for Metallo-Borophenes. *Angew. Chem. Int. Ed.* **2016**, *55* (26), 7358−7363.

(25) Popov, I. A.; Jian, T.; Lopez, G. V.; Boldyrev, A. I.; Wang, L.-S. Cobalt-centred boron molecular drums with the highest coordination number in the CoB_{16}^- cluster. *Nat. Commun.* **2015**, *6* (1), 8654.

(26) Jian, T.; Li, W.-L.; Popov, I. A.; Lopez, G. V.; Chen, X.; Boldyrev, A. I.; Li, J.; Wang, L.-S. Manganese-centered tubular boron cluster − MnB_{16}^-: A new class of transition-metal molecules. *J. Chem. Phys.* **2016**, *144* (15), 154310.

(27) Li, W.-L.; Jian, T.; Chen, X.; Li, H.-R.; Chen, T.-T.; Luo, X.-M.; Li, S.-D.; Li, J.; Wang, L.-S. Observation of a metal-centered B_2-Ta@B_{18}^- tubular molecular rotor and a perfect Ta@B_{20}^- boron drum with the record coordination number of twenty. *Chem. Commun.* **2017**, *53* (10), 1587−1590.

(28) Li, W.-L.; Chen, T.-T.; Jiang, Z.-Y.; Chen, W.-J.; Hu, H.-S.; Wang, L.-S.; Li, J. Probing the electronic structure of the CoB_{16}^- drum complex: Unusual oxidation state of Co^{-1}. *Chin. J. Chem. Phys.* **2019**, *32* (2), 241−247.

(29) Chen, T.-T.; Li, W.-L.; Chen, W.-J.; Yu, X.-H.; Dong, X.-R.; Li, J.; Wang, L.-S. Spherical trihedral metallo-borospherenes. *Nat. Commun.* **2020**, *11* (1), 2766.
(30) Romanescu, C.; Galeev, T. R.; Li, W.-L.; Boldyrev, A. I.; Wang, L.-S. Aromatic Metal-Centered Monocyclic Boron Rings: Co©B_8^- and Ru©B_9^-. *Angew. Chem. Int. Ed.* **2011**, *50* (40), 9334−9337.
(31) Li, W.-L.; Romanescu, C.; Galeev, T. R.; Piazza, Z. A.; Boldyrev, A. I.; Wang, L.-S. Transition-Metal-Centered Nine-Membered Boron Rings: M©B_9 and M©B_9^- (M = Rh, Ir). *J. Am. Chem. Soc.* **2012**, *134* (1), 165−168.
(32) Romanescu, C.; Galeev, T. R.; Sergeeva, A. P.; Li, W.-L.; Wang, L.-S.; Boldyrev, A. I. Experimental and computational evidence of octa- and nona-coordinated planar iron-doped boron clusters: Fe©B_8^- and Fe©B_9^-. *J. Organomet. Chem.* **2012**, *721*−*722*, 148−154.
(33) Chen, T.-T.; Li, W.-L.; Bai, H.; Chen, W.-J.; Dong, X.-R.; Li, J.; Wang, L.-S. Re©B_8^- and Re©B_9^-: New Members of the Transition-Metal-Centered Borometallic Molecular Wheel Family. *J. Phys. Chem. A* **2019**, *123* (25), 5317−5324.
(34) Galeev, T. R.; Romanescu, C.; Li, W.-L.; Wang, L.-S.; Boldyrev, A. I. Observation of the Highest Coordination Number in Planar Species: Decacoordinated Ta©B_{10}^- and Nb©B_{10}^- Anions. *Angew. Chem. Int. Ed.* **2012**, *51* (9), 2101−2105.
(35) Li, W.-L.; Romanescu, C.; Piazza, Z. A.; Wang, L.-S. Geometrical requirements for transition-metal-centered aromatic boron wheels: The case of VB_{10}^-. *Phys. Chem. Chem. Phys.* **2012**, *14* (39), 13663−13669.
(36) Heine, T.; Merino, G. What Is the Maximum Coordination Number in a Planar Structure? *Angew. Chem. Int. Ed.* **2012**, *51* (18), 4275−4276.
(37) Barroso, J.; Pan, S.; Merino, G. Structural transformations in boron clusters induced by metal doping. *Chem. Soc. Rev.* **2022**, *51* (3), 1098−1123.
(38) Chen, X.; Zhao, Y.-F.; Wang, L.-S.; Li, J. Recent progresses of global minimum searches of nanoclusters with a constrained Basin-Hopping algorithm in the TGMin program. *Comput. Theor. Chem.* **2017**, *1107*, 57−65.
(39) Zhao, Y.; Chen, X.; Li, J. TGMin: A global-minimum structure search program based on a constrained basin-hopping algorithm. *Nano Res.* **2017**, *10* (10), 3407−3420.
(40) Chen, X.; Zhao, Y.-F.; Zhang, Y.-Y.; Li, J. TGMin: An efficient global minimum searching program for free and surface-supported clusters. *J. Comput. Chem.* **2019**, *40* (10), 1105−1112.
(41) Frisch, M. J.; Trucks, G. W.; Schlegel, H. B.; Scuseria, G. E.; Robb, M. A.; Cheeseman, J. R.; Scalmani, G.; Barone, V.; Petersson, G. A.; Nakatsuji, H.; Li, X.; Caricato, M.; Marenich, A. V.; Bloino, J.; Janesko, B. G.; Gomperts, R.; Mennucci, B.; Hratchian, H. P.; Ortiz, J. V.; Izmaylov, A. F.; Sonnenberg, J. L.; Williams-Young, D.; Ding, F.; Lipparini, F.; Egidi, F.; Goings, J.; Peng, B.; Petrone, A.; Henderson, T.; Ranasinghe, D.; Zakrzewski, V. G.; Gao, J.; Rega, N.; Zheng, G.; Liang, W.; Hada, M.; Ehara, M.; Toyota, K.; Fukuda, R.; Hasegawa, J.; Ishida, M.; Nakajima, T.; Honda, Y.; Kitao, O.; Nakai, H.; Vreven, T.; Throssell, K.; Montgomery, J. E., Jr.; Peralta, J. E.; Ogliaro, F.; Bearpark, M. J.; Heyd, J. J.; Brothers, E. N.; Kudin, K. N.; Staroverov, V. N.; Keith, T. A.; Kobayashi, R.; Normand, J.; Raghavachari, K.; Rendell, A. P.; Burant, J. C.; Iyengar, S. S.; Tomasi, J.; Cossi, M.; Millam, J. M.; Klene, M.; Adamo, C.; Cammi, R.; Ochterski, J. L.; Martin, R. L.; Morokuma, K.; Farkas, O.; Foresman, J. B.; Fox, D. J. *Gaussian 16*, Revision A.03; Gaussian, Inc.: Wallingford CT, 2016.
(42) Perdew, J. P.; Burke, K.; Ernzerhof, M. Generalized Gradient Approximation Made Simple. *Phys. Rev. Lett.* **1996**, *77* (18), 3865−3868.
(43) Peterson, K. A.; Figgen, D.; Dolg, M.; Stoll, H. Energy-consistent relativistic pseudopotentials and correlation consistent basis sets for the 4d elements Y−Pd. *J. Chem. Phys.* **2007**, *126* (12), 124101.
(44) Dunning, T. H., Jr. Gaussian basis sets for use in correlated molecular calculations. I. The atoms boron through neon and hydrogen. *J. Chem. Phys.* **1989**, *90* (9), 1007−1023.
(45) Adamo, C.; Barone, V. Toward reliable density functional methods without adjustable parameters: The PBE0 model. *J. Chem. Phys.* **1999**, *110* (13), 6158−6170.
(46) Kendall, R. A.; Dunning, T. H., Jr.; Harrison, R. J. Electron affinities of the first-row atoms revisited. Systematic basis sets and wave functions. *J. Chem. Phys.* **1992**, *96* (9), 6796−6806.
(47) Weigend, F.; Ahlrichs, R. Balanced basis sets of split valence, triple zeta valence and quadruple zeta valence quality for H to Rn: Design and assessment of accuracy. *Phys. Chem. Chem. Phys.* **2005**, *7* (18), 3297−3305.
(48) Michalak, A.; Mitoraj, M.; Ziegler, T. Bond Orbitals from Chemical Valence Theory. *J. Phys. Chem. A* **2008**, *112* (9), 1933−1939.
(49) Mitoraj, M. P.; Michalak, A.; Ziegler, T. A Combined Charge and Energy Decomposition Scheme for Bond Analysis. *J. Chem. Theory Comput.* **2009**, *5* (4), 962−975.
(50) Te Velde, G.; Bickelhaupt, F. M.; Baerends, E. J.; Fonseca Guerra, C.; van Gisbergen, S. J. A.; Snijders, J. G.; Ziegler, T. Chemistry with ADF. *J. Comput. Chem.* **2001**, *22* (9), 931−967.
(51) Fenn, J. B.; Mann, M.; Meng, C. K.; Wong, S. F.; Whitehouse, C. M. Electrospray Ionization for Mass Spectrometry of Large Biomolecules. *Science* **1989**, *246* (4926), 64−71.
(52) Fonseca Guerra, C.; Snijders, J. G.; te Velde, G.; Baerends, E. J. Towards an order-N DFT method. *Theor. Chem. Acc.* **1998**, *99* (6), 391−403.
(53) Zubarev, D. Y.; Boldyrev, A. I. Developing paradigms of chemical bonding: adaptive natural density partitioning. *Phys. Chem. Chem. Phys.* **2008**, *10* (34), 5207−5217.
(54) Glendening, E. D.; Landis, C. R.; Weinhold, F. Natural bond orbital methods. *WIREs Comput. Mol. Sci.* **2012**, *2* (1), 1−42.
(55) Schleyer, P. V. R.; Maerker, C.; Dransfeld, A.; Jiao, H.; van Eikema Hommes, N. J. R. Nucleus-Independent Chemical Shifts: A Simple and Efficient Aromaticity Probe. *J. Am. Chem. Soc.* **1996**, *118* (26), 6317−6318.
(56) Stanger, A. Reexamination of $NICS_{\pi,zz}$: Height Dependence, Off-Center Values, and Integration. *J. Phys. Chem. A* **2019**, *123* (17), 3922−3927.
(57) Lu, T.; Chen, F. Multiwfn: A multifunctional wavefunction analyzer. *J. Comput. Chem.* **2012**, *33* (5), 580−592.
(58) Li, W.-L.; Ivanov, A. S.; Federič, J.; Romanescu, C.; Černušák, I.; Boldyrev, A. I.; Wang, L.-S. On the way to the highest coordination number in the planar metal-centred aromatic Ta©B_{10}^- cluster: Evolution of the structures of TaB_n^- (n = 3−8). *J. Chem. Phys.* **2013**, *139* (10), 104312.
(59) Li, J.; Bursten, B. E. Electronic Structure of Cycloheptatrienyl Sandwich Compounds of Actinides: An(η^7-C_7H_7)$_2$ (An = Th, Pa, U, Np, Pu, Am). *J. Am. Chem. Soc.* **1997**, *119* (38), 9021−9032.
(60) Liu, Z.; Lu, T.; Chen, Q. An sp-hybridized all-carboatomic ring, cyclo[18]carbon: Electronic structure, electronic spectrum, and optical nonlinearity. *Carbon* **2020**, *165*, 461−467.
(61) Wang, X.-B.; Wang, L.-S. Observation of negative electron-binding energy in a molecule. *Nature* **1999**, *400* (6741), 245−248.
(62) Wang, X.-B.; Wang, L.-S. Experimental Search for the Smallest Stable Multiply Charged Anions in the Gas Phase. *Phys. Rev. Lett.* **1999**, *83* (17), 3402−3405.
(63) Wang, X.-B.; Ferris, K.; Wang, L.-S. Photodetachment of Gaseous Multiply Charged Anions, Copper Phthalocyanine Tetrasulfonate Tetraanion: Tuning Molecular Electronic Energy Levels by Charging and Negative Electron Binding. *J. Phys. Chem. A* **2000**, *104* (1), 25−33.
(64) Wang, X.-B.; Wang, L.-S. Photodetachment of Multiply Charged Anions: The Electronic Structure of Gaseous Square-Planar Transition Metal Complexes PtX_4^{2-} (X = Cl, Br). *J. Am. Chem. Soc.* **2000**, *122* (10), 2339−2345.
(65) Dreuw, A.; Cederbaum, L. S. Multiply Charged Anions in the Gas Phase. *Chem. Rev.* **2002**, *102* (1), 181−200.
(66) Simons, J. Molecular Anions. *J. Phys. Chem. A* **2008**, *112* (29), 6401−6511.

https://doi.org/10.1021/acs.inorgchem.3c04636
Inorg. Chem. 2024, 63, 6276−6284

(67) Wang, X.-B.; Wang, L.-S. Photoelectron Spectroscopy of Multiply Charged Anions. *Annu. Rev. Phys. Chem.* **2009**, *60* (1), 105−126.
(68) Wang, L.-S. Perspective: Electrospray photoelectron spectroscopy: From multiply-charged anions to ultracold anions. *J. Chem. Phys.* **2015**, *143* (4), 040901.

https://doi.org/10.1021/acs.inorgchem.3c04636
Inorg. Chem. 2024, 63, 6276−6284